Three-Dimensional Structure of AmpC β-Lactamase from *Escherichia coli* Bound to a Transition-State Analogue: Possible Implications for the Oxyanion Hypothesis and for Inhibitor Design†

Ken C. Usher,‡,§ Larry C. Blaszczak, G. Scott Weston,|| Brian K. Shoichet,*,|| and S. James Remington*,‡

Institute of Molecular Biology, University of Oregon, Eugene, Oregon 97403, Infectious Disease Research, Lilly Research Laboratories, Eli Lilly & Co., Lilly Corporate Center, Indianapolis, Indiana 46285, and Department of Molecular Pharmacology and Biological Chemistry, Northwestern University, Chicago, Illinois 60611-3008

Received May 21, 1998

ABSTRACT: The structures of AmpC β-lactamase from *Escherichia coli*, alone and in complex with a transition-state analogue, have been determined by X-ray crystallography. The native enzyme was determined to 2.0 Å resolution, and the structure with the transition-state analogue *m*-aminophenylboronic acid was determined to 2.3 Å resolution. The structure of AmpC from *E. coli* resembles those previously determined for the class C enzymes from *Enterobacter cloacae* and *Citrobacter freundii*. The transition-state analogue, *m*-aminophenylboronic acid, makes several interactions with AmpC that were unexpected. Perhaps most surprisingly, the putative "oxyanion" of the boronic acid forms what appears to be a hydrogen bond with the backbone carbonyl oxygen of Ala318, suggesting that this atom is protonated. Although this interaction has not previously been discussed, a carbonyl oxygen contact with the putative oxyanion or ligand carbonyl oxygen appears in most complexes involving a β-lactam recognizing enzyme. These observations may suggest that the high-energy intermediate for amide hydrolysis by β-lactamases and related enzymes involves a hydroxyl and not an oxyanion, although the oxyanion form certainly cannot be discounted. The involvement of the main-chain carbonyl in ligand and transition-state recognition is a distinguishing feature between serine β-lactamases and serine proteases, to which they are often compared. AmpC may use the interaction between the carbonyl of Ala318 and the carbonyl of the acylated enzyme to destabilize the ground-state intermediate, this destabilization energy might be relieved in the transition state by a hydroxyl hydrogen bond. The structure of the m-aminophenylboronic acid adduct also suggests several ways to improve the affinity of this class of inhibitor and points to the existence of several unusual binding-site-like features in the region of the AmpC catalytic site.

β-lactamases catalyze the hydrolysis of the lactam bond of β-lactam antibiotics, inactivating these compounds (Figure 1). These enzymes are expressed by a wide variety of bacteria. They have been grouped into four classes: A, B, C, and D, which differ from each other in mechanism, size, substrate preferences, and inhibition patterns (*1*). Atomic resolution structures have been determined for enzymes from class A (*2*−*6*), class C (*7, 8*), and class B (*9*); the differences and similarities between these structures have been reviewed (*10, 11*). These enzymes are the major resistance mechanism to β-lactam antibiotics such as the penicillins and the cephalosporins. β-lactam antibiotics are widely used and historically have been very effective. The emergence of β-lactamase-mediated resistance is an important and growing threat to human health (*12, 13*).

† This work was partly supported by the PhRMA foundation and by MCB-9734484 from the NSF (to B.K.S.) and by MCB-9728162 from the NSF (to S.J.R.). K.C.U. was partly supported by a grant from Eli Lilly & Co. (to S.J.R.).

* Corresponding authors. E-mail: (B.K.S.) b-shoichet@nwu.edu, (S.J.R.) jim@uoxray.moregon.edu.

‡ University of Oregon.

§ Current address: Howard Hughes Medical Institute, UT Southwestern Medical Center, 5323 Harry Hines Blvd., Dallas TX 75235.

|| Eli Lilly & Co.

The mechanism of action of β-lactamases has been widely studied (*2, 3, 14*−*23*). Like proteases, β-lactamases catalyze the hydrolysis of an amide bond (Figure 1). The task is at once easier and harder for β-lactamases than it is for proteases. The four-membered β-lactam ring is strained, reducing the intrinsic stability of the amide bond (*23, 24*). Conversely, the amide is part of a ring, and when the nitrogen leaves after nucleophilic attack, it is still attached to the molecule and cannot diffuse away. This reduces the ability of water to hydrolyze the serine ester due to steric and electrostatic hindrance. Unlike the amide substrates of proteases, it is deacylation and not acylation that is either rate limiting (*25, 26*) or jointly rate limiting (*15*) for serine β-lactamases. The ability of β-lactamases to deacylate rapidly from the ester intermediate distinguishes them from penicillin-binding proteins (PBPs), which are the principal targets of β-lactam antibiotics in the bacterial cell and from which the serine β-lactamases are thought to have evolved (*10, 27*).

The mechanism of the serine β-lactamases is best characterized for class A β-enzymes. The structure of a mutant of TEM-1 β-lactamase acylated with penicillin G (*3*), along with mutagenesis experiments (*20, 28, 29*), suggests that Glu166 is a key residue in deacylation. The structure of

10.1021/bi981210f CCC: $15.00
Published on Web 10/28/1998

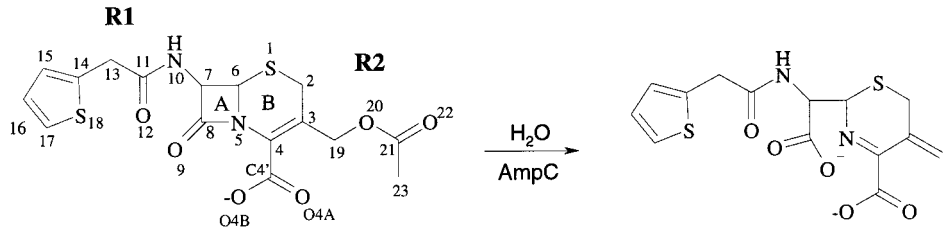

FIGURE 1: The hydrolysis of cephalothin to its inactive product. The A ring is the lactam or 2-azetidinone ring; the B ring is the dihydrothiazine ring. The R1 and R2 side chains are labeled.

the transition-state (TS) analogue [(*N*-(benzyloxycarbonyl)-amino)methyl]phosphonic acid bound to the class A β-lactamases from *Staph. aureus* (*18*) and to TEM-1 (*30*) have also been determined. These complexes are thought to resemble acylation high-energy intermediates. In a fourth structure, the positions of boronic acid oxygens from another transition-state analogue bound to TEM-1 β-lactamase are thought to resemble those of the oxygens attached to the tetrahedral center in a deacylation transition state (*21*). The position of the putative "oxyanion" is conserved in all three transition-state analogue complexes.

Structural studies have also advanced our understanding of class C enzymes, although here, the mechanism is less well understood. The structure of the class C enzyme from *Citrobacter freundii* in complex with aztreonam helped to confirm catalytic roles for amino acids Ser64, Lys67, Tyr150, and Lys315 and suggested roles for Asn152, Thr316, and Ser318 (*8*). The importance of these residues was borne out by structural studies of the class C enzyme from *Enterobacter cloacae*, in which a role was also observed for Gln120 (*7*). The structure of the *E. cloacae* enzyme covalently bound to the transition-state analogue *m*-carboxyphenyl[(*N*-((*p*-iodophenyl)acetyl)amino)methyl] phosphonate is thought to correspond to either an acylation or a deacylation high-energy intermediate (*19*). As was the case with the class A enzymes, the phosphonate group places one oxygen in the "oxyanion" hole of AmpC, which has been proposed to be formed by the main-chain nitrogens of Ser64 and residue 318 (Ala318 in AmpC from *Escherichia coli*, Ser318 in AmpC from *E. cloacae*) (*8, 19*). Unlike the class A β-lactamases, neither the identity nor the direction of attack of the deacylation water in the class C enzymes has been established. The identity of the catalytic base for the class C enzymes is also a matter of debate (*8, 19, 27, 31, 32*).

To characterize further the mechanism of the class C β-lactamases, we have determined the X-ray crystal structure of AmpC β-lactamase from *E. coli*, alone and in the presence of *m*-aminophenylboronic acid (MAPB)[1] (Figure 2). Like the phosphonate inhibitors, MAPB is considered to be a transition-state analogue (*33, 34*). The X-ray crystal structure of the MAPB−AmpC complex shows that this compound forms a bond with the catalytic Ser64 of AmpC, consistent with the proposed mechanism of inhibition. MAPB makes several unexpected interactions that speak to our understanding of the mechanism of serine β-lactamases. The structure of the complex also suggests possibilities for further inhibitor design against AmpC, which is a target for antiresistance drug discovery.

[1] Abbreviations: MAPB, *m*-aminophenylboronic acid; rms, root-mean-square; NCS, noncrystallographic symmetry; DMSO, dimethyl sulfoxide; K_I, inhibition constant, MNPB, *m*-nitroboronic acid.

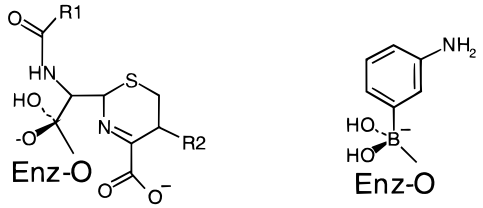

FIGURE 2: A structure for the high-energy tetrahedral intermediate along the deacylation pathway for AmpC and that of the MAPB-adduct with AmpC.

MATERIALS AND METHODS

E. coli AmpC was produced from plasmid POGO295 in the JM109 strain of *E. coli*. The ampC gene is under the control of a temperature-sensitive repressor in this plasmid, and protein production was initiated by heating a cell culture in LB broth with 10 mg/L tetracycline (OD_{600} of 0.2) from 37 to 41 °C. The cells were incubated at this temperature overnight, and on harvesting had reached an OD_{600} of 1.7. The cells were separated from the supernatant by two centrifugation steps at 10 000 rpm in a JA-14 rotor (30 min at 4 °C). The supernatant was adjusted to pH 7 using Tris base and was run over an *m*-aminophenylboronic acid Affigel-10 affinity column (*34*). The column was washed with 20 mM Tris, pH 7, and 0.5 M NaCl until no protein was observed in the eluent. AmpC was eluted by passing 0.5 M boric acid, pH 7.0, over the column. The enzyme was more than 97% homogeneous by HPLC. AmpC was concentrated by ultrafiltration, and the boric acid was removed by dialysis against 50 mM phosphate buffer, pH 6.8. The enzyme was either lyophilized and stored at −12 °C or was stored in 0.02% sodium azide and 50 mM phosphate, pH 6.8 at 4 °C.

AmpC crystals were grown by vapor diffusion and microseeding techniques, using the hanging drop method over 1.7 M sodium/potassium phosphate well solution, pH 8.5−8.7. The protein was reconstituted with distilled water from a lyophilized stock to make a 10 mg/mL solution, which was then mixed with an equal volume of phosphate well solution. Unsilanized glass coverslips were used initially to nucleate growth of small crystals, which were under 100 μm in size and usually twinned. These crystals were subsequently crushed and diluted with phosphate solution to make seed crystals. Single crystals up to 800 × 500 × 200 μm grew when a hair was dragged first through the seed solution then through a new vapor diffusion droplet. Lower protein concentrations (2−5 mg/mL) and silanized glass coverslips were used in those setups. Crystals with MAPB (Sigma) bound were grown by microseeding as above, but with the inhibitor premixed with the protein solution at a concentration of 1 mM so that it would cocrystallize bound to the enzyme.

Table 1: Data Collection Statistics

	native AmpC	MAPB
unit cell		
a (Å)	117.7	119.4
b (Å)	77.4	79.0
c (Å)	99.3	99.0
β (deg)	116.5	116.3
resolution range (highest shell)[a] (Å)	25−2.0 (2.25−2.0)[a]	25−2.3 (2.48−2.3)[a]
unique reflections observed (highest shell)	40 898 (9094)[a]	35 225 (6468)[a]
unique reflections calculated (highest shell)	52 822 (15650)[a]	36 886 (7324)[a]
data completeness	77.4% (58.1%)[a]	95.4% (88.3%)[a]
no. of observations	73 349	114 023
mean $I/\sigma(I)$	10.8 (3.1)[a]	10.1 (2.7)[a]
R-merge	7.0% (18.3%)[a]	8.8% (21.6%)[a]

[a] Values in parentheses are for the highest resolution shell used in refinement.

Table 2: Refinement Statistics

	native AmpC	MAPB
resolution range (Å)	25−2.0	25−2.3
rmsd bond lengths (Å)	0.019	0.019
rmsd bond angles (deg)	2.8	2.7
rmsd *B*-value correlations (Å^2)	7.7	8.0
crystallographic *R*-factor (%)	21.8	15.9
no. of solvent molecules	85	110

The cell dimensions and space group were determined initially by means of precession photos. Native data were collected on an R-Axis-II image plate system from a crystal that was frozen at 100 K and processed using software from Molecular Structures Corporation. This crystal was soaked for 3 h total in mother liquor with progressively more glycerol added, to a final glycerol content of 25%, then flash-frozen in a gaseous nitrogen cold stream. Data on a MAPB-containing crystal were collected at room temperature on a Xuong-Hamlin multiwire detector and processed using the supplied software (*35*).

A model based on the coordinates of AmpC from *E. cloacae* (*7*) was used to obtain a molecular replacement solution of the *E. coli* enzyme presented here. The search model was essentially the same as entry 2BLT in the Brookhaven Protein Data Bank (PDB) but was obtained from Professor J. Knox prior to its general release. Since the sequences of AmpC from *E. cloacae* and from *E. coli* share 81% identity, the search model included the side chains of all conserved residues, with alanines substituted at the positions of the nonconserved residues. The molecular replacement search was performed using the program AMoRe (*36*). A rotational search of the Patterson function was followed by two translational searches, first for one monomer and then for a second monomer in the asymmetric unit, keeping the position of the first monomer fixed.

Changes in the structure were modeled graphically using the program O (*37*), alternating with cycles of automated least-squares refinement performed using TNT release 5F (*38*), including NCS restraints of the two monomers in the asymmetric unit.

Enzyme assays were performed with cephalothin as provided by the manufacturer (Sigma). The hydrolysis reaction was monitored at 265 nm in a Hewlett-Packard 8453 diode array spectrophotometer. Assays were run in 50 mM potassium phosphate, pH 7.0, and 100 mM potassium chloride. Enzyme concentrations were typically 6.6×10^{-5} mg/mL, established using an extinction coefficient of 2.45 OD/mg/mL/cm. This extinction coefficient was determined using the method of Gill and von Hippel (*39*). The inhibitors MAPB (Sigma) and *m*-nitrophenylboronic acid (MNPB, Lancaster) were used as provided by the manufacturers. The inhibitors were dissolved in DMSO stock solutions and diluted into the assay buffer. DMSO concentrations were never more than 3%; at these concentrations, DMSO alone had no measurable effect on the uninhibited reaction rates.

RESULTS

The atomic model from *E. cloacae* was used as the basis for a molecular replacement solution for the *E. coli* AmpC structure. At the end of the fitting stage of the molecular replacement solution, using the two molecules in the asymmetric unit and data from 10 to 3.5 Å resolution, the correlation coefficient was 0.72, and the crystallographic R-factor was 32.6%. The electron density calculated with that solution was of very good quality and clearly showed the missing AmpC side chains. Phase combination with SIRAS phases obtained from a platinum-soaked derivative was done prior to model coordinate refinement and verified that there were no major differences between the two structures (data not shown). Data collection and refinement statistics for the final models of the native *E. coli* AmpC structure at 2.0 Å resolution and of the MAPB-bound structure at 2.3 Å resolution are reported in Tables 1 and 2. The crystallographic coordinates for both the native AmpC and the MAPB-bound complex have been submitted to the PDB (accession codes 2BLS and 3BLS, respectively).

AmpC from *E. coli* has a mixed α/β secondary structure, with a nine-stranded antiparallel β-sheet in the middle, flanked by a row of three α-helices on one side, and a helical domain with 11 helices on the other. The overall structure of AmpC from *E. coli*, reported here, is very similar to those previously reported for AmpC from *C. freundii* (*8*) and from *E. cloacae* (*7*). The enzyme also resembles class A β-lactamases, although it is about 100 amino acids larger, with four identifiable insertions, as previously described (*7*).

Structural similarity between *E. coli* and *E. cloacae* AmpC was expected, since there is 81% sequence identity between the two enzymes, and this is borne out in comparisons between final refined models of the two proteins. The Cα atoms of the A monomers from each of the respective asymmetric units overlay within 0.45 Å over 356 amino acids (excluding 1 and 4 residues from the N-terminus of the *E. coli* and *E. cloacae* models, respectively). Although the

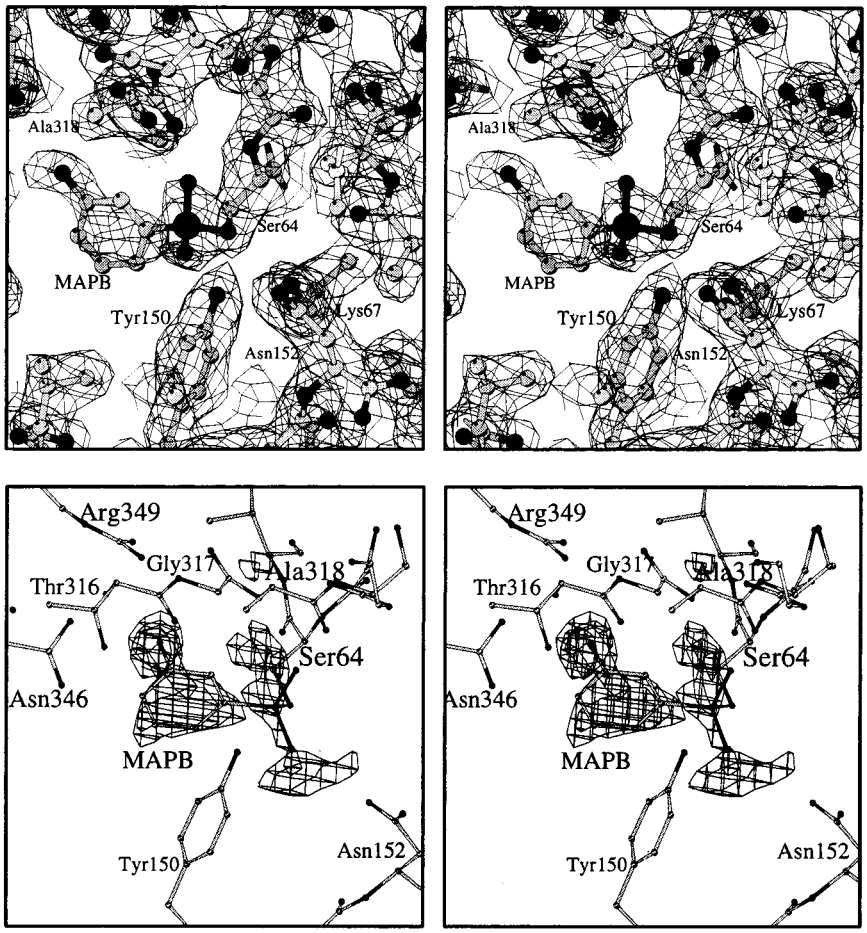

FIGURE 3: MAPB inhibitor electron density (stereo), displayed using the program Bobscript (*55*). (a) $2F_o - F_c$ electron density, contoured at 1 σ, of the fully refined MAPB complex, including the inhibitor atoms. Heteroatoms are dark gray, the carbon atoms are light gray. The boron atom is labeled (B). (b) Positive $F_o - F_c$ difference electron density in active site, contoured at 2.5 σ, after *xyz* refinement of protein atoms against MAPB data, before addition of any inhibitor atoms. Inhibitor model is displayed for reference only.

crystal packing and space groups are different, the *E. coli* and *E. cloacae* AmpC crystals both have two monomers in the asymmetric unit, allowing some comparisons of internal variance. In the case of *E. coli*, both monomers were refined with NCS restraints, producing rms differences of 0.22−0.24 Å over all Cα atoms, while in the *E. cloacae* models, where NCS restraints reportedly were not used, the rms differences over all Cα atoms were only 0.18−0.22 Å (*7*).

The primary catalytic residue of AmpC is Ser64, which is acylated in the course of β-lactam hydrolysis. Other active-site residues include Lys67, Gln120, Tyr150, Asn152, Lys315, Thr316, and the backbone of Ala318, whose main-chain nitrogen participates with that of Ser64 to form the putative "oxyanion" hole of AmpC. These active site residues are completely conserved in class C β-lactamases except for Ala318, which is sometimes a serine, but it is the backbone of that residue which forms part of the active site. Optimal overlay of the coordinates of all atoms of these seven residues between the *E. coli* and *E. cloacae* AmpC models results in an rms deviation of 0.75 Å. Visual examination of all residues within 10 Å of Ser64 also reveals no significant changes in either backbone or side-chain conformations between the two models, implying that the two active sites are functionally highly similar.

The structure of the complex between MAPB and AmpC is consistent with the status of boronic acids as transition-state analogues (*21*, *33*). Clear electron density connects the Oγ of the catalytic Ser64 to the boron atom of the boronic acid, suggesting a covalent bond has formed (Figure 3a). The disposition of groups around the boron atom is tetrahedral. In Figure 3b, $F_o - F_c$ difference electron density is shown in the region where MAPB binds. Figure 3a shows $2F_o - F_c$ electron density for the refined model, including inhibitor. The MAPB inhibitor makes a number of favorable interactions with the protein (Table 3, Figure 4). Atoms within hydrogen-bonding distance of MAPB include the N of Ser64, and the N and O atoms of Ala318, which interact with one of the boronic oxygens (O1). An apparent hydrogen bond is also observed between the meta-amino group of MAPB and the Asn346 side chain. The hydroxyl of Tyr150 is 3.2 Å from the C6 atom of the MAPB phenyl ring. There are also nonpolar contacts between the rings of

Table 3: Key Polar Contacts in AmpC/MAPB Complex

AmpC residue	atom	MAPB atom	distance[a] (Å)
Ser64	N	O1	3.0 (3.3)
Ala318	N	O1	2.9 (2.9)
Ala318	O	O1	2.6 (2.6)
Tyr150	OH	O2	4.1 (3.8)
Tyr150	OH	Ser64 Oγ	2.7 (2.9)
Tyr150	OH	Lys315 Nζ	3.0 (3.0)
Tyr150	OH	Lys67 Nζ	3.2 (3.4)
Asn346	OD1	NH2	3.1 (2.9)

[a] The distances given are for monomer B of the AmpC−MAPB complex. The distances observed in monomer A are in parentheses.

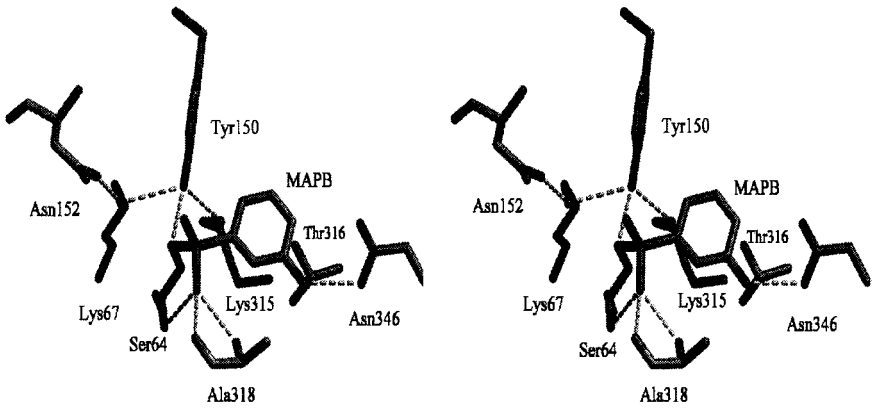

FIGURE 4: The residue environment of MAPB (stereo). Key hydrogen bonds (Table 2) are shown as dashed lines.

MAPB and Tyr150, with distances from C6 of MAPB and Tyr Cϵ1 of 3.6 Å (monomer B; A, 3.9 Å) and Cζ of 3.7 Å (A, 3.8 Å).

Comparison of the refined structures of *E. coli* AmpC with no ligand and that of AmpC with MAPB bound shows that neither the active-site residues nor the protein as a whole change much. The rms deviation between the atoms in the six active site residues listed above is 0.32 Å (for monomer A from each structure), hardly more than the 0.22 Å (native) and 0.28 Å (MAPB) rms deviations when monomers A and B of the same structure are compared. Similarly, the rms deviation for all protein atoms is 0.6 Å between the native and the MAPB complex structures (monomer A), compared with 0.46 Å (native) and 0.35 Å (MAPB) for all protein atoms between monomers in the same crystal.

Enzyme Inhibition. Two boronic acid inhibitors, MAPB and MNPB, inhibit AmpC without measurable delay; incubation times up to 20 min have no effect on the level of inhibition. MAPB and MNPB inhibit the enzyme competitively and reversibly, allowing us to determine inhibition constants that reflect the energy of binding. These constants were determined using the Lineweaver−Burk plots for MNPB and by using progress curves (*33*) for MNPB and MAPB. For MNPB, the Lineweaver−Burk analysis suggested a K_i value of 1.7 μM and the progress curve analysis suggested a K_i value of 1.2 $\pm$ 0.1 μM. The K_i value for MAPB was 7.3 $\pm$ 0.9 μM using the progress curve method.

DISCUSSION

Two aspects of the complexes between AmpC and MAPB stand out. First, an unexpected close contact is observed between the putative "oxyanion" of MAPB (the O1 atom of MAPB) and the carbonyl oxygen of Ala318, suggesting that the O1 is protonated. Second, the structure of the AmpC site suggests opportunities for further non-β-lactam inhibitor discovery against this antiresistance target. We will first consider the unexpected interaction with the O1 of MAPB and the carbonyl of Ala318 and then return to discuss possible areas for inhibitor discovery.

Perhaps the most surprising aspect of the MAPB complex is the close contact between the putative oxyanion (O1) of MAPB and the carbonyl oxygen of Ala318. In the structure, these two atoms are 2.6 Å apart (Table 3, Figures 4 and 5a). This distance suggests that the O1 boronic oxygen is either protonated or is making strongly repulsive interactions with the enzyme. Given the micromolar and submicromolar affinities of MAPB and its congeners (*40*), the latter hypothesis seems unlikely. The O1 oxygen is probably not an oxyanion but is rather a hydroxyl. Since the boronic adduct bears a formal negative charge in the tetrahedral adduct, the self-energy of the boronic acid will strongly favor a neutral hydroxyl over an oxyanion. Binding interactions also favor a hydroxyl, which can form an additional hydrogen bond with the enzyme. In this complex, both boronic acid chemistry and the geometry of the site favor a protonated form of the inhibitor.

What is harder to explain is that the interaction between the carbonyl oxygen of residue 318 (residue 237 in the class A β-lactamases) can also be observed in five of six other β-lactamase−ligand complex structures whose structures were available to us (Table 4, Figures 5 and 6). In two of these complexes (complexes 2 and 3 in Table 4), where the ligand is a boronic or a phosphonic acid transition-state analogue, the ligand oxygen has been proposed to be an oxyanion. In three others, the ligand oxygen is a carbonyl. In the case of the boronic acid complex with TEM-1 (complex 3, Table 4) (*21*), the close contact between the putative "oxyanion" and the main-chain oxygen of the enzyme is consistent with the O1 oxygen being protonated. As with the MAPB−AmpC complex, both boron chemistry and site geometry favor the protonated form of the boronic acid O1. In contrast to the boronic acid complexes, the low pK_a of the acidic oxygen in the phosphonate complexes may counterbalance the favorable hydrogen bonding potential of the protonated form of the inhibitor. If the phosphonic acid adducts do exist in their anionic form, the geometry of the complex suggests that the anions will have high-energy (unfavorable) interactions with the backbone carbonyl of residue 318/237. In the B-monomer of the phophonate complex with the AmpC from *E. cloacae* (complex 2, Table 4) the distance between the oxyanion and the carbonyl oxygen is 2.9 Å, making this interaction particularly unfavorable; here too, the geometry favors a hydroxyl form. In the A-monomer of this complex and in the phosphonate adduct with class A β-lactamase from *Staph. aureus* (complex 4, Table 4), the distance between the ligand O1 and the carbonyl oxygen is 3.4 Å, attenuating this unfavorable energy. Even so, the geometries are consistent with an electrostatic interaction between the two atoms. The pK_a values of the substrate oxygens in the high-energy intermediates is unknown, but based on model hemiketals (*41*) and hemiacetals (*42*), the pK_a value is likely to be no lower than 9 and is

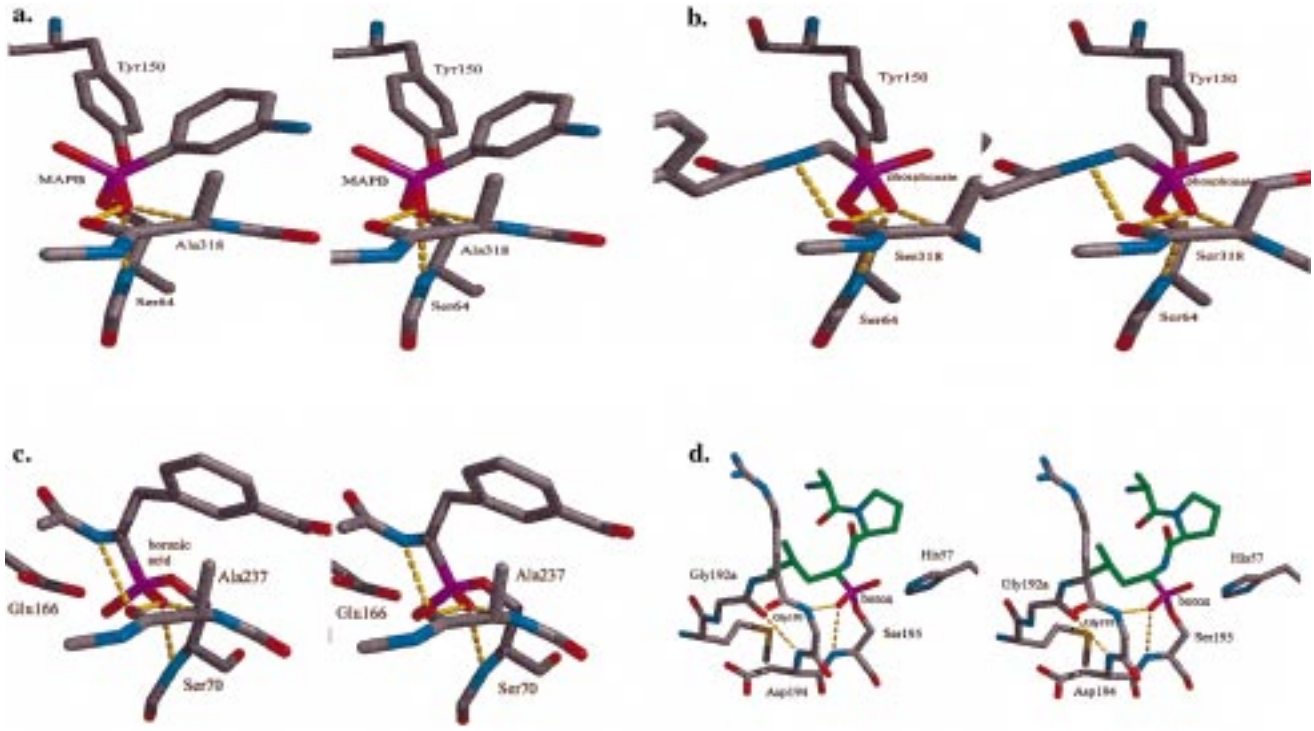

FIGURE 5: Comparing the interactions of β-lactamases with transition-state analogues to those of a serine protease with a transition-state analogue. Carbon atoms are in gray, oxygen atoms are in red, and nitrogens are in blue. Polar interactions between heavy atoms that are 2.6−3.1 Å apart (hydrogen bonds) are drawn as yellow dashed lines. (a) The MAPB−AmpC (*E. coli*) adduct. (b) The phosphonate−AmpC (*E. cloacae*) adduct (*19*). (c) The boronic acid TEM-1 adduct (*21*). (d) The complex between a boronic acid peptide and alpha-lytic protease (*47*); ligand carbon atoms are in green. Unlike the complexes in panels a−c, no interaction is observed between the ligand O1 oxygen and an enzyme carbonyl oxygen in the serine protease structure.

Table 4: Distances from the Carbonyl Oxygen of Residue 318, 237, or 301 in β-lactamases and a PBP with the Ligand "oxyanion"

	enzyme	inhibitor	main-chain oxygen of residue	distance to ligand oxygen[a] (Å)	torsion angle[b]	angle[c]
1	*E. coli* AmpC	boronic acid	318	2.6 (2.6)[d]	20°	141°
2	*Ent. cloacae*	phosphonate	318	2.9 (3.4)[d]	2°	122°
3	*E. coli* TEM-1	boronic acid	237	2.9	20°	133°
4	*S. aureus* P99	phosphonate	237	3.4	55°	122°
5	*E. coli* TEM-1	penicillin G	237	2.9	23°	31°
6	*E. coli* TEM-1	6α-hydroxy-methylpenicillanic acid	237	2.9	23°	31°
7	*S. aureus* dd-peptidase	cephalothin	301	2.8	33°	124°

[a] The oxygen occupying the putative "oxyanion" binding site (e.g., the O1 oxygen in the boronic acid and phosphonate complexes). [b] The torsion angle is measured from residue 318, 237, or 301, as appropriate, and is the angle defined by Cα to C to O to the inhibitor oxygen (e.g., the O1 oxygen of the boronic acid or phosphonate complexes. The best torsion for a hydrogen bond would be 0°. [c] The angle defined by the boron, phosphorus, or carbon atom of the inhibitor, the "oxyanion" and the interacting carbonyl oxygen (e.g., in the MAPB complex this would be boron to O1 to O of Ala315). The best angle for a hydrogen bond would be about 105°. [d] Monomer two in asymmetric unit.

probably higher; thus, a protonated O1 would be reasonable based on acidity. Of course, the environment of the active sites of serine β-lactamases and PBP enzymes might perturb these pK_a values, as occurs in serine proteases. Experiments to examine the effects of site environment on pK_as have not been conducted, to our knowledge, in a β-lactam-recognizing enzyme. All that can be said at this point is that the pK_a values of the substrates in solution do not intrinsically discount the idea of a hydrogen bond interaction in the high-energy intermediate, rather the opposite. The structures of complexes involving serine β-lactamases suggest that it may be possible for the substrate to adopt a protonated, hydroxyl form in the high-energy intermediate. We return to consider caveats to this argument below.

In the acyl−enzyme complexes with substrates (complexes 5−7 in Table 4), the carbonyl of the substrate also appears to make a close, polar contact with a backbone carbonyl of the enzyme (residue 318, 237, and 301 in the class C enzymes, the class A enzymes, and the DD-peptidase, respectively). Such a close contact should be energetically unfavorable, and may imply ground-state destabilization of the acylated state. Unlike the putative oxyanion−carbonyl interaction in the transition state, such a high-energy contact in the acylated ground state could be catalytically favorable in a mechanism where deacylation is rate limiting (*25*, *26*). This will be the case if the destabilizing interaction is attenuated in the deacylation transition state (i.e., if the free-energy difference, $\Delta G^{\ddagger}$, between the ground state and the transition state is reduced by the destabilization of the ground state).

The oxyanion hypothesis is well established for serine proteases. Two backbone amide-NHs stabilize the oxyanion

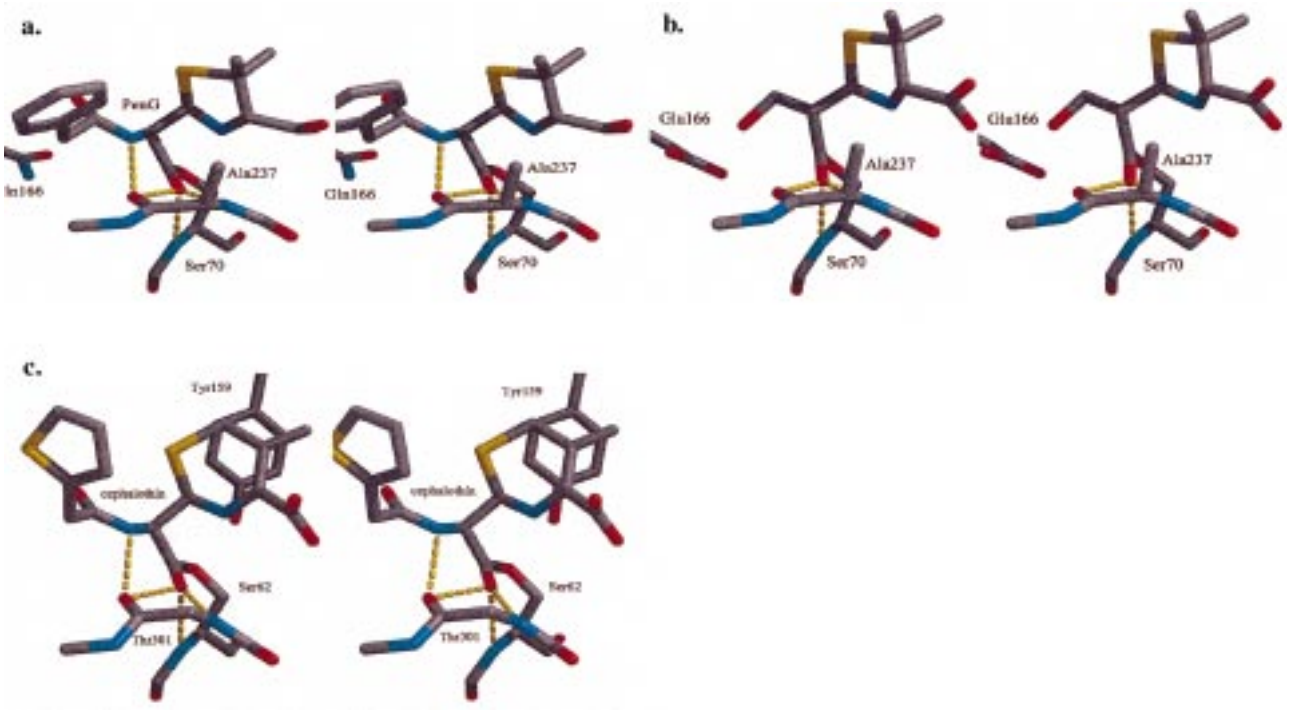

FIGURE 6: Interactions between serine β-lactamas recognizing enzymes and their acyl adducts. Colors as in Figure 5. (a) The penicillin-G adduct with TEM-1 (*3*). (b) The 6-α-hydroxymethylpenicillanic acid adduct with TEM-1 (*27*). (c) The cephalothin adduct with the R61 D-ala-D-ala hydrolase from *Streptomyces* (*10*).

of the high-energy tetrahedral intermediates by forming hydrogen bonds. In β-lactamases, hydrogen bonds also have been observed between the ligand oxygen and two backbone nitrogens, those of Ser64 (Ser70) and Ala/Ser318 (Ala/Gln237). The apparent similarity between these interactions and sites has led to the proposal that serine β-lactamases share the same oxyanion-stabilization mechanism that operates in serine proteases. However, the interaction distances presented here suggest that hydroxyl binding may be possible in the β-lactamase site due to the proximity of a nearby backbone carbonyl oxygen that acts as a hydrogen bond acceptor. Such a carbonyl oxygen is not present in the oxyanion hole of serine proteases. The "oxyanion" hypothesis for serine β-lactamases has been widely accepted (*23*, *43*) and appeals to one's sense of mechanistic conservation. It is appropriate to consider the detailed geometries represented in the crystal structures in attempting to distinguish between a hydroxyl and an oxyanion.

Are the angles of interaction consistent with hydrogen bond formation between the ligand "hydroxyl" and the carbonyl oxygen of residue 318/237? Similarly, are the angles between the carbonyl oxygens of the acylated intermediates and that of residue 318/237 consistent with a high-energy, destabilizing contact? For optimal interaction with the lone pair of the main-chain carbonyl oxygen, one would expect the O1 atom of the ligand to lie in the plane of the carbonyl system, at an angle of 120° to the C−O bond. For the boronic acid and phosphonate structures, the angle to this plane ranges 2−20° out of plane, and the angle to the C−O bond ranges 108−136°. These are well within allowed tolerances for hydrogen bonds (*44*). From the standpoint of the hydroxyl, one would expect the angle between the boron (or phosphorus) atom, the O1, and the O of the carbonyl to be about 110°. It is observed to range 122−141°. These deviations are within the range observed in macromolecular crystallography (*44*) and are less than observed between some canonical β-lactam-β-lactamase interactions, such as that between the R1 amide nitrogen of the ligand and the carbonyl oxygen of residue 318. Visually, the interaction between the O1 of the ligand and the carbonyl oxygen of the protein seems reasonable in each of the different complexes (Figures 5 and 6).

Does this observed close interaction necessarily imply hydrogen bonding or, in the case of carbonyl oxygen−carbonyl oxygen interaction, electrostatic repulsion? In several complexes, the main-chain oxygen (residue 318 or 237) is also involved in hydrogen bonding to the amide nitrogen of the substrate or substrate-analogue R1 side chain (N10 in Figure 1). It is possible that the carbonyl−carbonyl or carbonyl−"oxyanion" interaction may simply owe to the need for residue 318 (237) to both supply a hydrogen bond donor from the main-chain nitrogen and supply a hydrogen bond acceptor from the carbonyl oxygen to the R1 amide nitrogen of the ligand. Still, the interaction between two carbonyls or a carbonyl and an oxyanion would be expected to be repulsive and energetically costly. Also, the interaction is observed whether or not the R1 side-chain amide nitrogen is present (it is absent in the MAPB complex with AmpC and in the 6-α-hydroxymethylpenicillanic acid complex with TEM-1). MAPB binds to AmpC with micromolar affinity and has analogues that bind with nanomolar affinity (*40*). This of course does not prove that all enzyme interactions in this series of inhibitors are favorable, but it weighs against the idea of a high-energy (unfavorable) electrostatic contact.

The oxyanion hypothesis for β-lactamases is made by analogy to that of serine proteases. In serine proteases, there is direct evidence supporting the existence of an oxyanion high-energy intermediate (*41*, *45*, *46*). It is instructive to

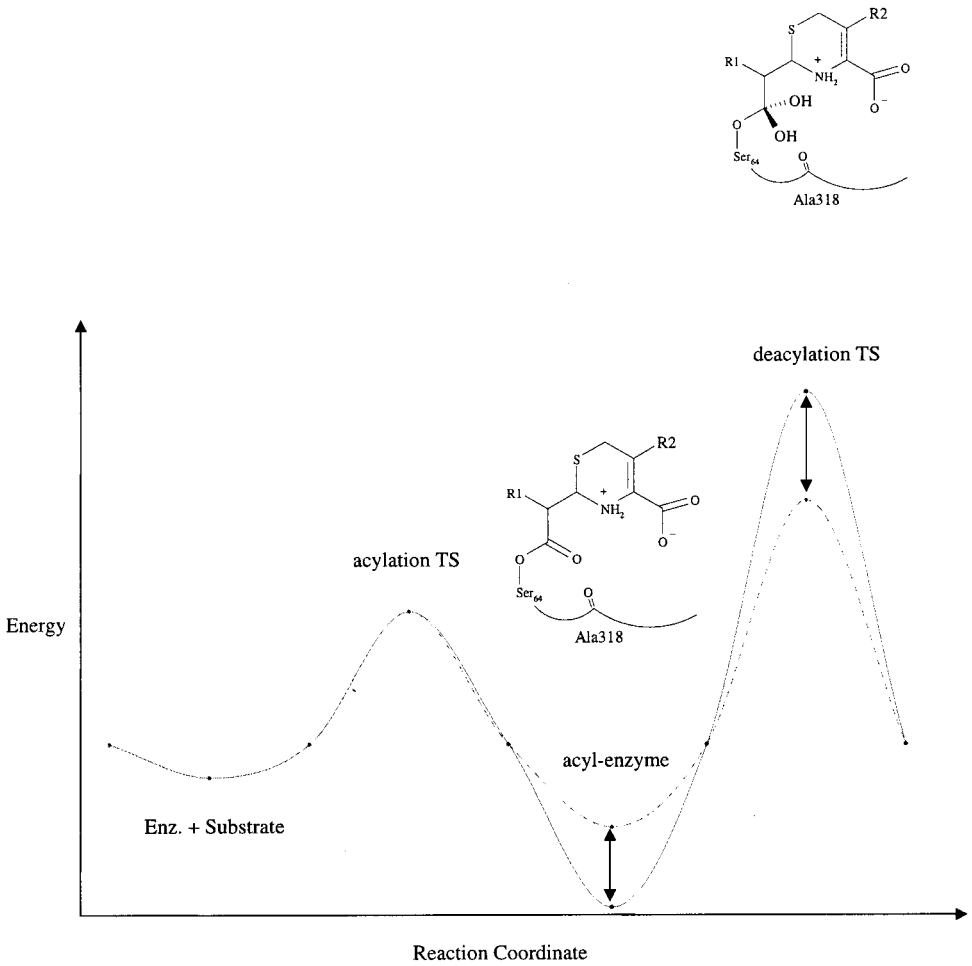

FIGURE 7: Cartoon of the reaction coordinate showing the effect of the proposed interaction with the carbonyl oxygen of residue 318 (237 in class A β-lactamases). These effects are represented by the dashed line, the solid line represents the case where the interactions with the carbonyl oxygen do not occur. In this model, the acyl−enzyme is destabilized by an unfavorable carbonyl oxygen−carbonyl oxygen interaction but the deacylation transition state is stabilized by a carbonyl oxygen−hydroxyl interaction. For clarity, the substates thought to exist with the acylation and deacylation transition states are not shown.

compare the oxyanion-binding site in serine proteases with that of β-lactamases. In serine proteases that adopt a chymotrypsin-like fold, the oxyanion hole is created by the main-chain nitrogens of Ser195 and Gly193, which are on the same strand. In the complex with a boronic acid and α-lytic protease (*47*) (Figure 5d), the nearest carbonyl oxygen to the boronic acid is that of Gly192, which is 4.0 Å away. This main-chain oxygen is involved in a hydrogen bond with the main-chain nitrogen of Asp194, suggesting that it is not directly interacting with the substrate oxyanion. The architecture of the serine proteases in this respect is quite different from that of the β-lactamases and PBP enzymes. In β-lactamases, the oxygen recognition main-chain nitrogens are drawn from amino acids widely separated in sequence, in different orientations than those found in the chymotrypsin family of serine proteases. The β-lactamase configuration is such as to recruit the participation of a backbone carbonyl in recognizing the high-energy intermediate oxygen.

Two caveats to the argument favoring a hydroxyl high-energy intermediate should be made. First, the source of the proton on the hydroxyl of the high-energy intermediate is unknown; invoking protonation adds an extra step to the mechanism. The crystal structures do not unambiguously identify the acid that would protonate the acyl-enzyme adduct. Second, although the boronic acid complexes with β-lactamases are the most likely to make hydrogen bond interactions with the carbonyl of residue 318 (237), these transition-state analogues also bear a negative charge in their adducts with the enzyme and, in that respect, resemble oxyanion high-energy intermediates.

Notwithstanding these caveats, it seems clear that β-lactamases differ significantly from serine proteases in the recognition of the tetrahedral high-energy intermediates. A reaction pathway that is consistent with the structural observations presented here may be constructed (Figure 7). Unlike serine proteases, the slow step in β-lactam hydrolysis for β-lactamases and PBPs is deacylation. On forming the acyl adduct, a high-energy contact occurs between the carbonyl oxygen of the substrate and that of Ala318. This contact destabilizes the intermediate ground state. This destabilization will reduce the energy difference ($\Delta G^{\ddagger}$) between this ground state and that of the deacylation high-energy intermediate that follows if this unfavorable interaction is absent in the transition state. In this model, the unfavorable carbonyl−carbonyl interaction would be converted into a favorable carbonyl−hydroxyl interaction in the deacylation tetrahedral intermediate. This would promote catalysis. This model may be tested by direct investigation of the protonation states of transition-state analogues (e.g.,

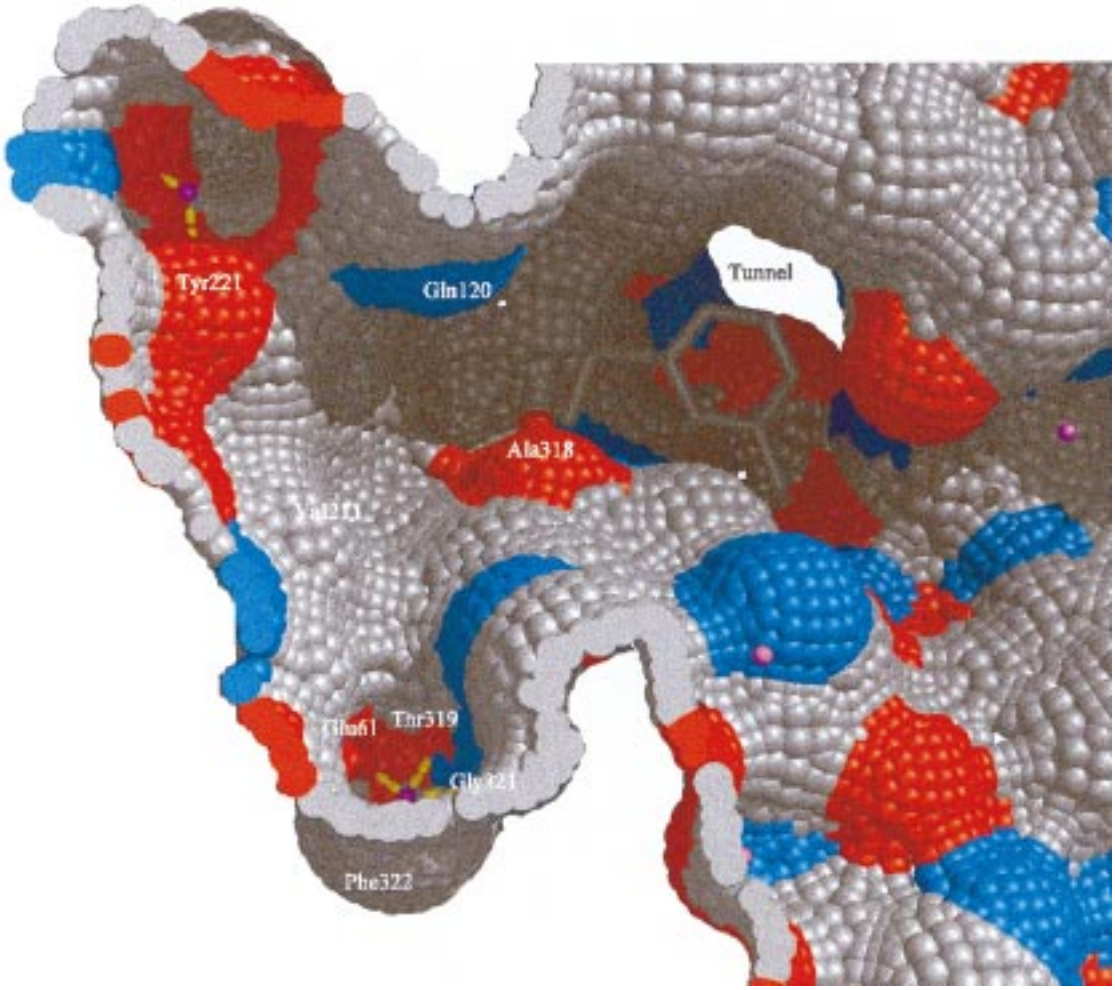

FIGURE 8: The molecular surface (*56*) of AmpC showing the catalytic and adjacent binding sites. MAPB is shown for reference. Carbon atom surface colored gray, oxygen atom surface red, and nitrogen atoms colored blue. Four ordered crystallographic water molecules are shown as magenta spheres; dashed yellow lines indicate hydrogen bonds to protein atoms. Several highly conserved residues are labeled. Figure generated using Neon in MidasPlus (*57*) and PaintShop Pro.

trifluoromethyl ketones), as took place with serine proteases (*41*, *45*).

Other Interactions and Applications to Inhibitor Design. Except for the O1 position and that of the boron, MAPB adopts a different orientation off of Ser64 than does the phosphonate inhibitor in the *E. cloacae* AmpC structure (*19*), exploring a different part of the AmpC-binding site (compare panels a and b of Figure 5). The aryl side chain makes several polar interactions with AmpC residues (Table 3). Asn346 makes a hydrogen bond with the amine of MAPB, the Oγ of Thr316 appears to make a dipole−quadrupole interaction with the phenyl ring (distance 2.8 and 3.4 Å from C4 in monomer A and B, respectively, with the Oγ 96° out of the phenyl ring plane). The hydroxyl of Tyr150 may interact similarly with the MAPB ring (distance to the ring carbon is 3.2 Å in both monomers, the angle to C6 is 42°).

Several of these interactions might be optimized by analogues of MAPB. The 3-nitro analogue MNPB has a K_i of 1.7 μM, 4-fold better than MAPB. This may be due to the improved complementarity to AmpC that occurs when the 3-amino group is replaced by the 3-nitro group [electrophilic activation of the boron by the nitro group cannot be discounted, but structure activity studies in this series suggest that this is not the only effect (*40*)]. The apparent dipole−quadrupole interaction involving Tyr150 might be improved by an analogue with a hydrogen bond acceptor in the 2-position of the ring; similar substitutions at the 4 position might improve interactions with Thr316 (*40*). The constancy of the AmpC conformation in crystal structures between different species (*7*, *8*) and in the presence or absence of different inhibitors (*19*) suggests that AmpC may provide a good template for structure-guided modifications of a lead inhibitor.

Several large-scale features of AmpC are worthy of note. The recognition site for the R1 side chain of cephalosporins and penicillins lies in the direction of Asn152 and Gln120 (*7*, *8*, *19*). This region has been an area of active exploration via syntheses of different R1 analogues of β-lactams. We note that this R1 site is large and contains several surface residues that are highly conserved and located in geometrically well-defined pockets, but for which no functions have been proposed. These residues include Glu61, Val211, Thr319, Tyr221, and Phe322 (Figure 8). Two regions that have been less explored border on the aryl side chain of MAPB. The 5 position of MAPB borders on the mouth of a tunnel that runs through the surface of the enzyme (Figure 8). This tunnel begins approximately at the Oγ of Thr316 and runs for 15 Å, emerging near residue Ser282. This tunnel also exists in the structure of the AmpC enzyme from *E. cloacae*. Several residues in this tunnel are highly

conserved among AmpC enzymes from different species. The 3-amino group of MAPB points toward a groove in the enzyme where several polar residues appear to point functionality into the same region of space. These residues include Asp288, Asn346, and Arg349, the polarity of which is well conserved among AmpC enzymes from different species. The roles that these sites might play in the catalytic mechanism of AmpC remain unclear (but see *48* and *8*); several undoubtedly have a role in recognizing the conserved carboxylate moiety of β-lactams as well as the R2 side chain. Several authors have proposed that AmpC may play a role in peptidoglycan synthesis or hydrolysis (*49*−*51*), and Pratt and colleagues have suggested that the enzyme possesses a secondary site for binding peptides (*52*−*54*). A role for these binding-site-like features in AmpC in recognizing non-β-lactam ligands cannot be excluded.

As tools for drug discovery, boronic acid inhibitors of AmpC have two applications. Boronic acids bind reversibly and rapidly to AmpC, allowing one to readily calculate binding affinities. In conjunction with structure determination, these affinities allow for the functional mapping of AmpC active sites, identifying complementary regions for other inhibitors. Also, boronic acids may themselves provide good beginnings for building tight-binding inhibitors (*40*). Such optimized derivatives may have potential as cotherapeutic agents to prevent the enzymatic hydrolysis of β-lactam antibiotics, resensitizing resistant bacteria to these drugs.

CONCLUSIONS

The structure of AmpC from *E. coli* in complex with MAPB reveals several unexpected features. Perhaps most surprising among them is the observed interaction between the O1 oxygen of the boronic acid adduct and the carbonyl main-chain oxygen of Ala318. Such an interaction is observed in most other β-lactamase−inhibitor complexes. This interaction allows for the possibility that in the tetrahedral high energy intermediates along the hydrolytic pathway, what has been considered to be a substrate oxyanion may be protonated. The structures of serine β-lactamases differ from serine proteases in the juxtaposition of an enzyme main-chain carbonyl in the immediate vicinity of the putative oxyanion hole. This may suggest, although it certainly does not prove, that β-lactamases have a fundamentally different mechanism for recognizing tetrahedral high-energy intermediates than do chymotrypsin-like proteases, which have been the model enzymes to which they were compared.

ACKNOWLEDGMENT

The authors are grateful to Jean-Pierre Wery and Richard Clawson for early crystallographic work on AmpC, including an initial molecular replacement solution, and to Natalie Strynadka for providing the structure of TEM-1 bound to PenG. B.K.S. thanks Shariar Mobashery and Joanne Stubbe for enlightening conversations and Mark Cunningham for reading this manuscript.

REFERENCES

1. Bush, K., Jacoby, G. A., and Medeiros, A. A. (1995) *Antimicrob. Agents Chemother. 39*, 1211−1233.
2. Herzberg, O., and Moult, J. (1987) *Science 236*, 694−701.
3. Strynadka, N. C. J., Adachi, H., Jensen, S. E., Johns, K., Sielecki, A., Betzel, C., Sutoh, K., and James, M. N. G. (1992) *Nature 359*, 700−705.
4. Dideberg, O., Charlier, P., Wery, J. P., Dehottay, P., Dusart, J., Erpicum, T., Frere, J. M., and Ghuysen, J. M. (1987) *Biochem. J. 245*, 911−913.
5. Knox, J. R., and Moews, P. C. (1991) *J. Mol. Biol. 220*, 435−455.
6. Jelsch, C., Mourey, L., Masson, J. M., and Samama, J. P. (1993) *Proteins 16*, 364−383.
7. Lobkovsky, E., Moews, P. C., Liu, H., Zhao, H., Frere, J. M., and Knox, J. R. (1993) *Proc. Natl. Acad. Sci. U.S.A. 90*, 11257−11261.
8. Oefner, C., D'Arcy, A., Daly, J. J., Gubernatro, K., Charnas, R. L., and Winkler, F. K. (1990) *Nature 343*, 284−288.
9. Carfi, A., Pares, S., Euee, E., Galleni, M., Duez, C., Frere, J. M., and Dideberg, O. (1995) *EMBO J. 14*, 4914−4921.
10. Knox, J. R., Moews, P. C., and Frere, J. M. (1996) *Chem. Biol. 3*, 937−947.
11. Massova, I., and Mobashery, S. (1998) *Antimicrob. Agents Chem. 42*, 1−17.
12. Neu, H. C. (1992) *Science 257*, 1064−1073.
13. Davies, J. (1994) *Science 264*, 375−382.
14. Fisher, J., Belasco, J. G., Khosla, S., and Knowles, J. R. (1980) *Biochemistry 19*, 2895−2901.
15. Christensen, H., Martin, M. T., and Waley, S. G. (1990) *Biochem. J. 266*, 853−961.
16. Ellerby, L. M., Escobar, W. A., Fink, A. L., Mitchinson, C., and Wells, J. A. (1990) *Biochemistry 29* (24), 5797−5806.
17. Lamotte-Brasseur, J., Jacob-Dubuisson, F., Dive, G., Frere, J. M., and Ghuysen, J. M. (1992) *Biochem. J. 282*, 189−195.
18. Chen, C. C., J, J. R., Pratt, R. F., and Herzberg, O. (1993) *J. Mol. Biol. 234*, 165−78.
19. Lobkovsky, E., E. M.Bilings, Moews, P. C., Rahil, J., Pratt, R. F., and Knox, J. R. (1994) *Biochemistry 33*, 6762−6772.
20. Escobar, W. A., Miller, J., and Fink, A. L. (1994) *Biochem. J. 303*, 555−558.
21. Strynadka, N. C. J., Martin, R., Jensen, S. E., Gold, M., and Jones, J. B. (1996) *Nat. Struct. Biol*.
22. Zawadzke, L. E., Chen, C. C., Banerjee, S., Li, Z., Wasch, S., Kapadia, G., Moult, J., and Herzberg, O. (1996) *Biochemistry 35*, 16475−16482.
23. Galleni, M., Lamotte-Brassear, J., Raquet, X., Dubus, A., Monnaie, D., Knox, J. R., and Frere, J.-M. (1995) *Biochem. Pharmacol. 49*, 1171−1178.
24. Neuhaus, F. C., and Geogopapadakou, B. (1992) in *Emerging Targets for Antibacterial and Antifungal Chemotherapy* (Sutcliffe, J., and Geogopapadakou, N., Eds.) pp 206−273, Chapman & Hall, New York.
25. Pratt, R. F., McConnell, T. S., and Murphy, S. J. (1988) *Biochem. J. 254*, 919−922.
26. Knott-Hunziker, V., Petursson, S., SG, S. G. W., Jaurin, B., and Grundstrom, T. (1982) *Biochem. J. 207* (2), 315−322.
27. Bulychev, A., Massova, I., Miyashita, K., and Mobashery, S. (1997) *J. Am. Chem. Soc. 119*, 7619−7625.
28. Guillaume, G., Vanhove, M., Lamotte-Brasseur, J., Ledent, P., Jamin, M., Joris, B., and Frere, J. M. (1997) *J. Biol. Chem. 272*, 5438−5444.
29. Delaire, M., Lenfant, F., Labia, R., and Masson, J. M. (1991) *Protein Eng. 4*, 805−810.
30. Maveyraud, L., Pratt, R. F., and Samama, J.-P. (1998) *Biochemistry 37*, 2622−2628.
31. Dubus, A., Normark, S., Kania, M., and Page, M. G. (1994) *Biochemistry 33*, 8577−8586.
32. Dubus, A., Ledent, P., Lamotte-Brasseur, J., and Frere, J. M. (1996) *Proteins 25*, 473−485.
33. Beesley, T., Gascoyne, N., Knott-Hunziker, V., Petursson, S., Waley, S. G., Jaurin, B., and Grundstrom, T. (1983) *Biochem. J. 209*, 229−233.
34. Cartwright, S. J., and Waley, S. G. (1984) *Biochem. J. 221*, 505−512.
35. Howard, A. J., Neilsen, C., and Xuong, N. H. (1985) *Methods Enzymol. 114*, 452−472.

36. Navaza, J. (1994) *Acta Crystallogr. 50*, 157−163.
37. Jones, T. A., Zou, J. Y., Cowan, S. W., and Kjeldgaard, M. (1991) *Acta Crystallogr., Sect. A 47*, 110−119.
38. Tronrud, D. E., Eyck, L. F. T., and Matthews, B. W. (1987) *Acta Crystallogr., Sect. A 43*, 489−503.
39. Gill, S. C., and Hippel, P. H. v. (1989) *Anal. Biochem. 182*, 319−326.
40. Weston, G. S., Blazquez, J., Baquero, F., and Shoichet, B. K. (1998) (*submitted for publication*).
41. Liang, T. C., and Abeles, R. H. (1987) *Biochemistry 26*, 7603−7608.
42. Albert, A., and Sergeant, E. P. (1962) *Ionization Constants of Acids and Bases*, John Wiley & Sons, New York.
43. Murphy, B. P., and Pratt, R. F. (1988) *Biochem. J. 256*, 692−672.
44. Jeffrey, G. A., and Saenger, W. (1991) *Hydrogen Bonding in Biological Structures*, Springer-Verlag, Berlin.
45. Brady, K., Liang, T. C., and Abeles, R. H. (1989) *Biochemistry 28*, 9066−9070.
46. Bullock, T. L., Breddam, K., and Remington, S. J. (1996) *J. Mol. Biol. 255*, 714−725.
47. Bone, R., Frank, D., Kettner, C. A., and Agard, D. A. (1989) *Biochemistry 28*, 7600−7609.
48. Dubus, A., Normark, S., Kania, M., and Page, M. G. (1995) *Biochemistry 34*, 7757−7764.
49. Bishop, R. E., and Weiner, J. H. (1992) *FEBS Lett. 304*, 103−108.
50. Bishop, R. E., and Weiner, J. H. (1993) *FEMS Microbiol Lett. 114*, 349−354.
51. Henderson, T. A., Young, K. D., Denome, S. A., and Elf, P. K. (1997) *J. Bacteriol. 179*, 6112−6121.
52. Dryjanski, M., and Pratt, R. F. (1995) *Biochemistry 34*, 3569−3575.
53. Dryjanski, M., and Pratt, R. F. (1995) *Biochemistry 34*, 3561−3568.
54. Xu, Y., Soto, G., Hirsch, K. R., and Pratt, R. F. (1996) *Biochemistry 35*, 3595−3603.
55. Esnouf, R. M. (1997) *J. Mol. Graphics 15*, 133−138.
56. Connolly, M. L. (1983) *Science 221*, 709−713.
57. Ferrin, T. E., Huang, C. C., Jarvis, L. E., and Langridge, R. (1988) *J. Mol. Graph. 6*, 13−27.

BI981210F